THE JOURNAL OF BIOLOGICAL CHEMISTRY VOL. 288, NO. 50, pp. 35801–35811, December 13, 2013

Structures of the *Bacillus subtilis* Glutamine Synthetase Dodecamer Reveal Large Intersubunit Catalytic Conformational Changes Linked to a Unique Feedback Inhibition Mechanism*

Received for publication, September 16, 2013, and in revised form, October 23, 2013 Published, JBC Papers in Press, October 24, 2013, DOI 10.1074/jbc.M113.519496

David S. Murray[‡], Nagababu Chinnam[§], Nam Ky Tonthat[§], Travis Whitfill[§], Lewis V. Wray, Jr.[¶], Susan H. Fisher[¶], and Maria A. Schumacher[§1]

From the [‡]Department of Biochemistry and Molecular Biology, Oregon Health and Science University, Portland, Oregon 97239, the [§]Department of Biochemistry, Duke University School of Medicine, Durham, North Carolina 27710, and the [¶]Department of Microbiology, Boston University School of Medicine, Boston, Massachusetts 02118

Background: *B. subtilis* GS catalyzes the production of glutamine, a key metabolite in nitrogen assimilation.
Results: *B. subtilis* GS forms a dodecamer that undergoes large intersubunit conformational changes during catalysis.
Conclusion: *B. subtilis* GS structures reveal a heretofore unseen active site restructuring that is linked to a novel feedback regulatory mechanism.
Significance: The GS specific regulatory/catalytic mechanism may be used to target Gram-positive pathogens.

Glutamine synthetase (GS), which catalyzes the production of glutamine, plays essential roles in nitrogen metabolism. There are two main bacterial GS isoenzymes, GSI-α and GSI-β. GSI-α enzymes, which have not been structurally characterized, are uniquely feedback-inhibited by Gln. To gain insight into GSI-α function, we performed biochemical and cellular studies and obtained structures for all GSI-α catalytic and regulatory states. GSI-α forms a massive 600-kDa dodecameric machine. Unlike other characterized GS, the *Bacillus subtilis* enzyme undergoes dramatic intersubunit conformational alterations during formation of the transition state. Remarkably, these changes are required for active site construction. Feedback inhibition arises from a hydrogen bond network between Gln, the catalytic glutamate, and the GSI-α-specific residue, Arg^{62}, from an adjacent subunit. Notably, Arg^{62} must be ejected for proper active site reorganization. Consistent with these findings, an R62A mutation abrogates Gln feedback inhibition but does not affect catalysis. Thus, these data reveal a heretofore unseen restructuring of an enzyme active site that is coupled with an isoenzyme-specific regulatory mechanism. This GSI-α-specific regulatory network could be exploited for inhibitor design against Gram-positive pathogens.

Glutamine is a key metabolite in nitrogen assimilation because it is not only incorporated into proteins but also serves as the direct nitrogen donor for the synthesis of nearly 25% of all nitrogen-containing compounds (1). Glutamine is synthesized from ammonium, ATP, and glutamate by the enzyme glutamine synthetase (GS).[2] Underscoring its essential role in nitrogen metabolism and assimilation, GS is found in all organisms and is tightly regulated (2–3). GS enzymes are all large homo-oligomeric machines, in which each active site is formed between subunit interfaces (3–13). There are three different classes of GS enzymes, categorized as GSI, GSII, and GSIII (14). GSI enzymes are specific to prokaryotes and archaea and have thus far all been shown to be dodecamers (3, 7–14). GSII enzymes are decamers consisting of two stacked pentamer rings and are found in eukaryotes and soil-dwelling bacteria (4, 5). GSIII proteins are harbored in certain anaerobic bacteria and cyanobacteria and, like GSI enzymes, are dodecamers but are formed from hexamer-hexamer interactions different from those that form GSI oligomers (6).

Despite their distinct oligomeric arrangements, the active site and residues involved in catalysis are conserved in GS proteins, suggesting similar overall mechanisms. This enzymatic reaction can be divided into two steps, which are facilitated by either Mg^{2+} or Mn^{2+} (3, 15). In the first step, the ϵ-oxygen of the substrate glutamate attacks the γ-phosphorus of ATP to form a γ-glutamyl phosphate intermediate (16–21). In the second step, ammonia, formed by the deprotonation of an ammonium ion, attacks the reaction intermediate to produce glutamine (Fig. 1*A*). Because of their central role in metabolism, GSs have emerged as important chemotherapeutic targets. For example, the herbicide glufosinate-ammonium, which inhibits plant GS, has recently become commercially available, and research is under way for the development of compounds that selectively target the *Mycobacterium tuberculosis* GS (22). The

* This work was supported, in whole or in part, by National Institutes of Health Grants GM074815 (to M. A. S.) and GM051127 (to S. H. F.). This work was also supported by an M. D. Anderson Trust Fellowship and Burroughs Wellcome Career Development Award (to M. A. S.).
The atomic coordinates and structure factors (codes 4LNK, 4LNI, 4LNF, 4LNN, and 4LNO) have been deposited in the Protein Data Bank (http://wwpdb.org/).
[1] To whom correspondence should be addressed: Dept. of Biochemistry, Duke University School of Medicine, 255 Nanaline H. Duke, Box 3711, DUMC, Durham, NC 27710. Tel.: 919-684-9468; Fax: 919-684-8885; E-mail: Maria.Schumacher@duke.edu.

[2] The abbreviations used are: GS, glutamine synthetase; ASU, asymmetric unit; AMPPCP, adenosine 5′-(β,γ-methylene)triphosphate; Ni-NTA, nickel-nitrilotriacetic acid; Met-Sox, L-methionine-*S*-sulfoximine; Met-Sox-P, Met-Sox-phosphate; ITC, isothermal titration calorimetry; r.m.s., root mean square.

TABLE 1
Selected crystallographic data for GS structures

Structure	Apo-GS	GS·glutamate·AMPPCP	GS·transition state
Resolution (Å)	120.2–3.10	120.4–2.87	117.1–2.58
Space group	P1	$C222_1$	P1
Cell constants (Å)	$a = 110.0$	$a = 138.9$	$a = 110.0$
	$b = 138.4$	$b = 240.9$	$b = 141.6$
	$c = 138.7$	$c = 207.6$	$c = 142.1$
Cell constants (degrees)	$\alpha = 119.8$	$\alpha = 90.0$	$\alpha = 60.3$
	$\beta = 90.2$	$\beta = 90.0$	$\beta = 67.4$
	$\gamma = 93.9$	$\gamma = 90.0$	$\gamma = 76.2$
Overall R_{sym} (%)[a]	11.5 (43.6)[b]	5.0 (30.9)	5.76 (20.1)
Overall $I/\sigma(I)$	12.1 (1.8)	13.8 (2.5)	12.2 (3.4)
No. of total reflections	186475	239473	364805
% Complete	97.8 (98.2)	92.1 (92.0)	90.0 (90.4)
Refinement statistics			
R_{work}/R_{free} (%)[c]	21.7/26.7	19.5/23.6	20.3/23.2
r.m.s. deviation			
Bond angles (degrees)	1.30	1.33	1.12
Bond lengths (Å)	0.008	0.010	0.022

[a] $R_{sym} = \Sigma\Sigma|I_{hkl} - I_{hkl(j)}|/\Sigma I_{hkl}$, where $I_{hkl(j)}$ is observed intensity, and I_{hkl} is the final average value of intensity.
[b] Values in parentheses are for the highest resolution shell.
[c] $R_{work} = \Sigma||F_o| - |F_c||/\Sigma|F_o|$ and $R_{free} = \Sigma||F_o| - |F_c||/\Sigma|F_o|$, where all reflections belong to a test set of 5% randomly selected data.

design of pathogen-specific drugs would be greatly facilitated by structural and biochemical studies revealing any unique catalytic or regulatory mechanisms utilized by these enzymes. However, our understanding of bacterial GS isoenzyme structure and function has been limited.

GSI is the major bacterial enzyme, and phylogenetic analysis reveals two GSI subdivisions, GSI-α and GSI-β (14). There are no GSI-α structures thus far described. GSI-β structures are available for the *Escherichia coli*, *M. tuberculosis*, and *Salmonella typhimurium* proteins, and the current understanding of GS catalysis is largely based on early studies of structures obtained from soaking various substrates/products into GSI-β crystals (3, 7–13). These studies suggested that relatively small structural alterations in active site loops are involved in catalysis (3, 10). GSI-α enzymes are found in low G + C Gram-positive bacteria and some thermophilic bacteria. The best studied GSI-α is that from the model Gram-positive bacterium *Bacillus subtilis* (23–32). Interestingly, despite the fact that GSI-α and GSI-β share 35–41% sequence identity, their mechanisms of regulation are distinct. GSI-β enzymes are regulated by adenylylation of an active site tyrosine, whereas GSI-α activity is subject to feedback inhibition by the product, Gln, and to a lesser extent, AMP (23, 32–36).

Notably, the GS·Gln feedback-inhibited form of *B. subtilis* GSI-α performs an unexpected role in controlling the DNA-binding activity of two global regulatory factors, GlnR and TnrA (29–31). GlnR and TnrA have similar N-terminal DNA binding domains with putative Mer-like motifs; however, they have distinct C-terminal domains, which are targeted by GS·Gln. GS·Gln forms a complex with TnrA that prevents it from binding DNA, hence shutting off transcription of genes encoding nitrogen catabolic and scavenging enzymes (29). By contrast, GS·Gln acts as a chaperone to stabilize GlnR·DNA complexes, which allows it to repress expression of genes such as *glnA* (encoding GS) (31). Thus, *B. subtilis* GS serves as an enzyme, a chaperone, and a DNA binding coeffector. To gain insight into the functions of this unique, multitasking GS protein, we obtained structures of all GS catalytic and regulatory states and performed biochemical and *in vivo* studies.

EXPERIMENTAL PROCEDURES

Protein Purification, Crystallization, and Structure Determination—An artificial gene (codon optimized for *E. coli* expression) encoding the *B. subtilis* GS was obtained from Genscript Corp. (Piscataway, NJ) and subcloned into pET15b for protein expression. Gel filtration of GS species indicated a dodecameric oligomer. The His tag was removed for all structural and biochemical studies. Crystals were grown via hanging drop vapor diffusion at room temperature. *B. subtilis* apo-GS crystals were obtained by mixing the protein (40 mg/ml) at a 1:1 ratio with 40% 4-methyl-2,4-pentanediol and 200 mM $MgSO_4$ and inverting the drop over the reservoir solution. These crystals contain a dodecamer in the crystallographic asymmetric unit (ASU). To produce GS·glutamate·AMPPCP crystals, glutamate and AMPPCP were added to GS (at 40 mg/ml) to final concentrations of 5 mM, and the solution was mixed 1:1 with a reservoir of 15% PEG 8000, 0.1 M Hepes, pH 7.5, and 10 mM $MgCl_2$. These crystals contain a hexamer in the ASU, and the dodecamer is generated via symmetry.

GS·Met-Sox-P·ADP was produced by mixing GS with 5 mM $MgCl_2$, 5 mM ATP, and 5 mM L-methionine-*S*-sulfoximine (Met-Sox) for 1 h. This solution was then combined 1:1 with a crystallization reagent of 10% PEG 4000, 0.1 M Hepes, pH 7.5. These crystals contain a dodecamer in the ASU. Two crystal forms of GS·Gln were obtained. Form 1 was grown by mixing the GS·glutamine complex 1:1 with 40% 4-methyl-2,4-pentanediol and 100 mM $MgCl_2$. Form 2 was obtained using 10% PEG 8000, 0.1 M Tris, pH 8.0, 5 mM $MgCl_2$ as a crystallization solution. Form 1 contains a dodecamer in the ASU, whereas form 2 contains a hexamer (with the dodecamer generated by crystal symmetry). All x-ray intensity data were collected at 100 K at the Advanced Light Source beamline 8.3.1. The space group and cell parameters of each crystal are shown in Tables 1 and 2. Phases were determined first for the apo-GS form by molecular replacement, using the *M. tuberculosis* GS dodecamer as the search model. Several nonconserved loops were removed from the search model before molecular replacement. Refinement was carried out using the Crystallography and NMR Software pack-

TABLE 2
Selected crystallographic data for GS-Gln structures

	Form 1 (P1)	Form 2 (C2)
Structural data		
Resolution (Å)	119.0–2.95	61.9–2.90
Space group	P1	C2
Cell constants (Å)	$a = 112.0$	$a = 209.0$
	$b = 136.5$	$b = 138.9$
	$c = 137.7$	$c = 144.7$
Cell constants (degrees)	$\alpha = 119.8$	$\alpha = 90.0$
	$\beta = 90.2$	$\beta = 125.7$
	$\gamma = 93.4$	$\gamma = 90.0$
Overall R_{sym} (%)[a]	10.3 (37.3)[b]	8.0 (37.7)
Overall $I/\sigma(I)$	12.2 (2.0)	13.3 (2.1)
No. of total reflections	274,737	175,345
Percentage complete	96.1 (96.0)	98.8 (91.6)
Refinement statistics		
R_{work}/R_{free} (%)[c]	20.0/25.8	19.6/25.6
r.m.s. deviation		
Bond angles (degrees)	1.12	1.20
Bond lengths (Å)	0.022	0.009

[a] $R_{sym} = \Sigma\Sigma|I_{hkl} - I_{hkl(j)}|/\Sigma I_{hkl}$, where $I_{hkl(j)}$ is observed intensity and I_{hkl} is the final average value of intensity.
[b] Values in parentheses are for the highest resolution shell.
[c] $R_{work} = \Sigma\|F_o| - |F_c\|/\Sigma|F_o|$ and $R_{free} = \Sigma\|F_o| - F_c\|/\Sigma|F_o|$, where all reflections belong to a test set of 5% randomly selected data.

age (CNS) and PHENIX (37, 38). The models were all constructed with the modeling program O (39).

Enzyme, Kinetic, and in Vivo Assays—The *glnA*(*R62A*) mutant was constructed, and overexpression and purification of the mutant R62A GS were performed as described previously (40). Methods for the cultivation of bacteria in the minimal medium of Neidhardt *et al.* (41) have been described previously (42). All cultures contained 0.5% glucose, whereas the final concentration of all nitrogen sources was 0.2%. β-Galactosidase was assayed in crude extracts prepared from cells grown to mid-log growth phase (42). The reported β-galactosidase levels were corrected for the endogenous activity present in cells containing the promoterless *lacZ* fusion vectors integrated into the *amyE* gene. One unit of β-galactosidase activity produced 1 nmol of *o*-nitrophenol min^{-1}. The kinetic constants for glutamate, ATP, and hydroxylamine were measured by assaying the production of γ-glutamylhydroxamate (32). The ammonium K_m values were determined by measuring the production of inorganic phosphate that resulted from the hydrolysis of ATP as described (43). The inhibition of the Mg^{2+}-dependent biosynthetic reaction by glutamine, AMP, and Met-Sox were determined with glutamate and ATP concentrations of 150 and 18 mM, respectively.

Cooperativity Assays—To assay for GS cooperativity, mixed GS oligomers were produced. The two proteins that were used to produce the mixed dodecamer were the WT, active protein and an inactive GS(E304A/A305G) mutant. The mutant also contained an N-terminal 35 residue extension, which included a His tag, followed by a tobacco etch virus cleavage site and a hydrophilic region. This extension permitted the detection of mixed dodecamer populations by SDS-PAGE. The GS(E304A/A305G) protein was expressed as for WT and purified via Ni-NTA chromatography. The N-terminal His tag of WT GS was cleaved via thrombin, and the cleaved protein was isolated as the flow-through of a Ni-NTA column. This untagged WT protein was then mixed with the His-tagged GS(E304A/A305G) protein. The mixed sample was dialyzed in buffer containing 20 mM Tris, pH 7.5, 150 mM NaCl, and 2 M urea for 12 h. This urea treatment resulted in dodecamer dissolution and monomer formation. The sample was then dialyzed into a buffer containing 20 mM Tris, pH 7.5, 150 mM NaCl, and 5 mM $MgCl_2$ for 16 h with buffer changes at 4 and 8 h to allow dodecamer formation. The sample was subjected to Ni-NTA purification; the imidazole-eluted fractions were isolated and treated with tobacco etch virus protease to remove the His tag from the GS(E304A-A305G) protein. The digested sample was dialyzed into buffer containing 20 mM Tris, pH 7.5, 150 mM NaCl, and 5 mM $MgCl_2$ overnight and applied to a Ni-NTA column to remove any His tag peptide and uncleaved protein. The samples were run on SDS-PAGE to ensure that both proteins were present. The enzymatic activities of the mixed dodecamer were measured by following the production of γ-glutamylhydroxamate (19). The Mg^{2+}-dependent forward reaction was assayed in a final volume of 0.5 ml containing 0.05 M imidazole, pH 7.0, 100 mM sodium glutamate, 40 mM hydroxylamine, 100 mM $MgCl_2$, and 18 mM ATP. The Mn^{2+}-dependent forward reaction was measured in a final volume of 0.5 ml containing 0.05 M imidazole, pH 7.0, 100 mM sodium glutamate, 40 mM hydroxylamine, 7.5 mM $MnCl_2$, and 7.5 mM ATP. The Mn^{2+}-dependent reverse (transferase) reaction was assayed in 0.5 ml containing 20 mM sodium arsenate, 50 mM hydroxylamine, 40 mM glutamine, 2 mM ADP, 25 mM Tris, pH 7.5, 0.33 mM $MnCl_2$, and 0.4 M K_2SO_4. The purified enzymes were pretreated with 0.4 M K_2SO_4 before addition to the transferase reaction buffer (19). For the biosynthetic reactions, 1 unit of GS activity corresponds to the ATP-dependent formation of 1 nmol of γ-glutamylhydroxamate min^{-1}. In the transferase reaction, 1 unit of GS activity is the ADP-dependent formation of 1 nmol of γ-glutamylhydroxamate min^{-1}.

Circular Cichroism (CD) and ITC Studies—CD measurements in the far UV regions (190–260 nm) were performed with pre- and post-urea-treated WT GS, GS(E304A/A305G) and the mixed complex at 25 °C with a 1-mm path length. Each sample solution contained 300 mM NaF and 10 mM Tris, pH 7.5. The temperature of the sample was controlled with a PTC-348 WI Peltier block. ITC experiments were performed using a VP-ITC system with GS loaded in the sample cell and either AMP or AMPPCP loaded in the syringe. The nucleotides were titrated into the sample cell with GS at 25 °C, and the resulting isotherms were fitted with the Origin software.

RESULTS AND DISCUSSION

Structure Determinations of B. subtilis GS and Its Complexes—To deduce the structural mechanism of GSI-α catalysis and its regulation, *de novo* crystals were obtained of the apo-, substrate-bound, glutamine-bound, and transition state complex (Tables 1 and 2). The transition state structure was obtained by reacting GS with ATP and Met-Sox (see "Experimental Procedures"). GS phosphorylates Met-Sox in the presence of ATP to form the transition state analog, Met-Sox-P, which causes irreversible inhibition of the enzyme (44). The *B. subtilis* apo-GS structure was solved first by molecular replacement using the *M. tuberculosis* GSI-β structure, which is 41% identical to *B. subtilis* GS (see "Experimental Procedures"). The structure, refined to R_{work}/R_{free} values of 21.7%/26.7% 3.1 Å (Table 1),

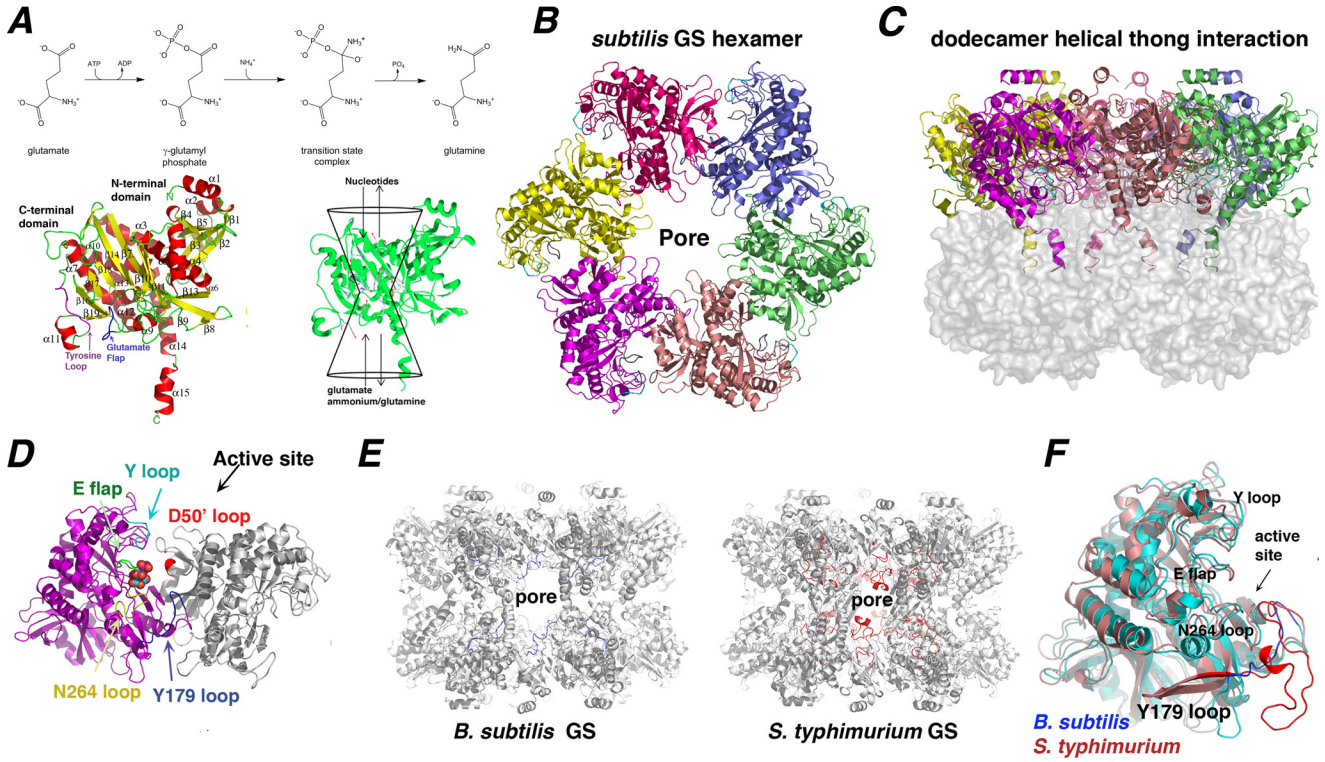

FIGURE 1. **Structure and enzymatic mechanism of *B. subtilis* GSI-α.** *A*, *top*, a scheme depicting the GS reaction mechanism. *Bottom left*, secondary structural elements of the GSI-α subunit. For reference, the Glu flap is *colored blue*, and the Tyr loop is *colored magenta*. *Ribbon diagrams* figures were made using PyMOL (47). *Bottom right*, the GS active site is illustrated as a bifunnel with entrance and exit portals. The glutamate and ATP substrates enter and bind at opposite ends of the bifunnel, and the respective products leave via the same portals. *B*, a hexamer of the dodecameric *B. subtilis* GS viewed down the molecular 6-fold axis. *C*, the GS dodecamer rotated by 90° relative to Fig. 1*B*. In this figure, the "bottom" hexamer is shown as a surface to highlight the interhexamer contacting α14-α15 helices. *D*, *close-up view* of an active site created by neighboring subunits. Key active site loops that line the active site are *labeled* and *colored differently*. A bound glutamate is shown in *CPK*. *E*, comparison of GS dodecamers of the *B. subtilis* GSI-α and *S. typhimurium* GSI-β proteins. Shown in *different colors* (*B. subtilis* in *blue* and *S. typhimurium* in *red*) are the active site Tyr^{179} loops that line the dodecameric pore (*labeled*). *F*, superimposition of a *B. subtilis* subunit (*blue*) onto a *S. typhimurium* subunit (*red*), highlighting their strong structural correspondence except for the Tyr^{179} loop. The location of the pore is *labeled* in *B* and *E* for reference.

contains 444 residues/subunit and is composed of 19 β-strands and 15 α-helices. The subunit can be divided by helix α3 into a larger C-terminal domain and a smaller, N-terminal region (Fig. 1*A*). Two hexameric rings are formed from six GS subunits and stack to form a dodecamer (Fig. 1, *B* and *C*). The hexameric rings are held together primarily by interactions between C-terminal helices α14 and α15 and α14′ and α15′ (where a prime indicates the neighboring subunit).

Each subunit has the classical GS bifunnel structure, whereby key residues that mediate catalysis are located on loops that encapsulate the active site (3, 45, 46) (Fig. 1*A*). The active site regions are mainly located in the C-terminal domain, with the N-terminal domain of the adjacent subunit contributing one loop. Previous studies on GSI-β enzymes led to the designation of key active site loops (8). Based on homology with GSI-β proteins, the corresponding GSI-α active site loops within the C-domain are the Glu flap (*B. subtilis* residues 301–306), the Tyr loop (residues 365–373), the Asn loop (residues 231–242), and the Tyr^{179} loop (residues 148–158). The N-terminal domain provides the $Asp^{50'}$ loop (also called the "latch"), which contributes a key catalytic aspartic acid. In *B. subtilis*, this loop consists of residues 52–66, and the catalytic aspartic acid corresponds to $Asp^{53'}$ (Fig. 1*D*).

Analysis of the Apo-GS Structure—The Glu flap and latch are arguably the most critical GS active site loops because they contribute residues that are central for catalysis. The aspartic acid from the $Asp^{50'}$ loop abstracts a proton from ammonium to create ammonia, and the Glu flap harbors the catalytic base (Glu^{304} in *B. subtilis* GS), which abstracts a proton from the transition state to form glutamine and ADP. In the apo-GSI-α structure, the Glu flap is almost entirely disordered; only residues 301 and 306 are visible, and they display *B*-factors (average) > 100 $Å^2$ (Table 3). Glu flap flexibility is important because it permits facile substrate entry and product release. The Tyr loop, which contains the tyrosine that is adenylylated in GSI-β enzymes, is also disordered. A corresponding tyrosine (Tyr^{373}) is found in the *B. subtilis* GSI-α; however, studies have shown that it is not adenylylated, consistent with a different GSI-α regulatory mechanism (23). Aside from the Glu flap and Tyr loop, clear density is observed for the other active site regions in the GSI-α apo-structure, and with the exception of the Tyr^{179} loop, the catalytic regions of the GSI-α enzyme are similar in length to GSI-β proteins. In GSI-β enzymes, the Tyr^{179} loop contains 36 residues and extends from the active site into the central dodecamer channel, whereas in the GSI-α structure, this region consists of a short, 11-residue loop (Fig. 1, *E* and *F*) (3). When the Tyr^{179} region is excluded, the Cα atoms of the *B. subtilis* GS subunit can be superimposed onto those of *S. typhimurium* (Protein Data Bank entry 1f52) and *M. tuberculosis* (Protein Data Bank entry 2bvc) with root mean square

(r.m.s.) deviations of 1.3 and 1.5 Å, respectively. The altered structures of the Tyr^{179} loop in GSI-α compared with GSI-β lead to different pore structures for these enzymes. The function(s), if any, of the pores, however, is not known (Fig. 1*E*).

GSI-α-Substrate and Transition State Structures Reveal That Large Conformational Changes Are Required for Catalysis—To gain insight into the enzymatic mechanism employed by GSI-α enzymes, we determined the structure of GSI-α bound to the substrates glutamate and AMPPCP (which is a non-hydrolyzable ATP analog) to 2.87 Å (Table 1). The substrate glutamates and AMPPCP molecules bind at each end of the bifunnel. The glutamate substrates are located under the Glu flap. Although better ordered than the apo-structure the Glu flap residues in this structure, as well as the glutamate substrates, display high *B*-factors (*B*-factors (average) = 86.7 $Å^2$ for the glutamate substrates and 85.0 $Å^2$ for Glu flap residues) (Table 3). This suggests that the active site may become protected by Glu flap closure only during catalysis. The glutamate substrate peptide carboxyl and amide groups interact with Arg^{298} and His^{245}, whereas its side chain carboxyl interacts with a Mg^{2+} ion. The adenine moiety of the AMPPCP is sandwiched between the side chains of Arg^{331} and Tyr^{201}, whereas hydrogen bonds to the adenine N6, N1, and N7 atoms are provided by the carbonyl oxygen of Ile^{328} and the side chains of Ser^{249} and Ser^{329}. Interestingly, the phosphate groups of AMPPCP point away from the active site and are only contacted weakly by Lys^{44}. In fact, density is only observed for the α- and β-phosphates of the AMPPCP molecules. Hence, AMPPCP does not appear to bind GS productively, which is consonant with ITC data showing that GS binds AMPPCP with 100-fold lower affinity than AMP (Fig. 2). Comparisons of the substrate-bound and apo-GSI-α structures revealed that not only are the subunits and their corresponding active sites essentially unchanged upon substrate binding, but the dodecameric arrangement remains unaffected as well (superimposition of Cα atoms = 0.50–0.60 Å/subunit and 0.60 Å for all Cα atoms of the dodecamers) (Fig. 3, *A–D*).

Key active site residues are conserved in all classes of GS, suggesting a similar overall catalytic mechanism. According to this reaction scheme, ATP and glutamate first bind in the active site at each end of the bifunnel. The bound ATP γ-phosphate is polarized by the metal ions and an arginine residue (corresponding to *B. subtilis* GSI-α Arg^{316}), which facilitates nucleophilic attack by the bound glutamate substrate to yield γ-glutamyl phosphate (Fig. 3*A*). The next step in the reaction involves proton abstraction of ammonium by the $Asp^{50'}$ aspartic acid to create the ammonia. The ammonia then reacts with the γ-glutamyl phosphate to form the tetrahedral transition state. The final step is dissociation of the phosphate from the intermediate and concomitant abstraction of the proton from the γ-amino group of the intermediate by the Glu flap glutamate (*B. subtilis* Glu^{304}).

GSI-β structures have defined the residues and specific active site architecture optimal for catalysis (3). At first glance, the minimal shifts in the active site regions of the apo- and substrate-bound *B. subtilis* GS structures appear to suggest that GSI-α catalysis may also involve only moderate active site loop movements. However, close examination of the apo- and substrate-bound GSI-α active sites reveal that they lack an optimal

TABLE 3
***B*-Factor (average) for GS structure Glu flap residues and substrates**

Structure	Glu flap *B*(av)	Substrate *B*(av)
	$Å^2$	$Å^2$
Apo	>100	NA[a]
Glutamate-bound	85	86.7
Transition state	24.0	20.1
Glutamine-bound	35.9	33.0

[a] Not applicable.

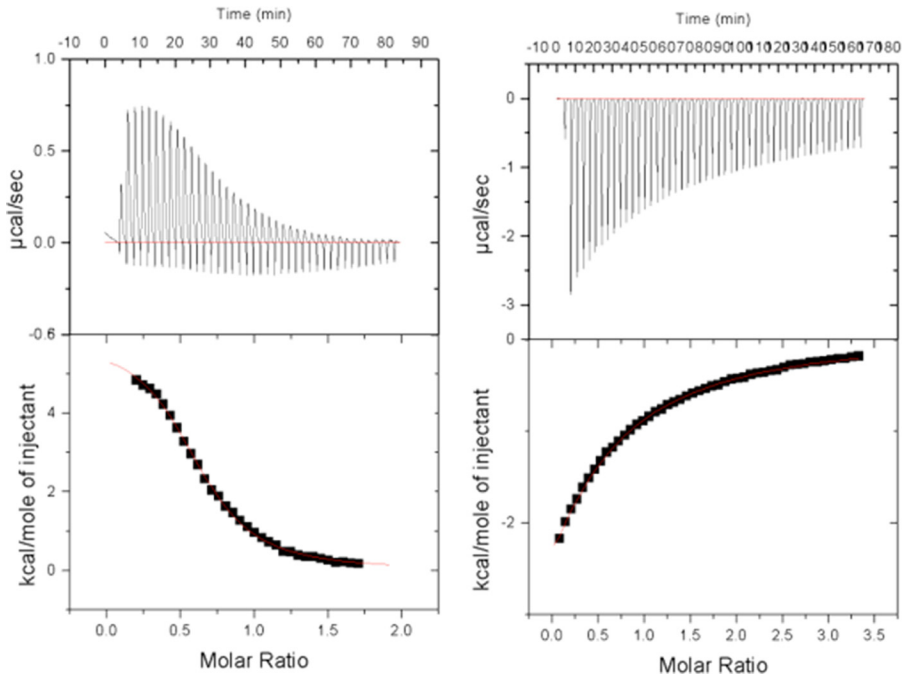

FIGURE 2. **Isothermal titration calorimetry thermograms of AMP and AMPPCP binding to GS.** *A*, AMP binding to GS. K_d = 7.5 ± 0.3 μM. *B*, AMPPCP binding to GS. K_d = 667 ± 21 μM.

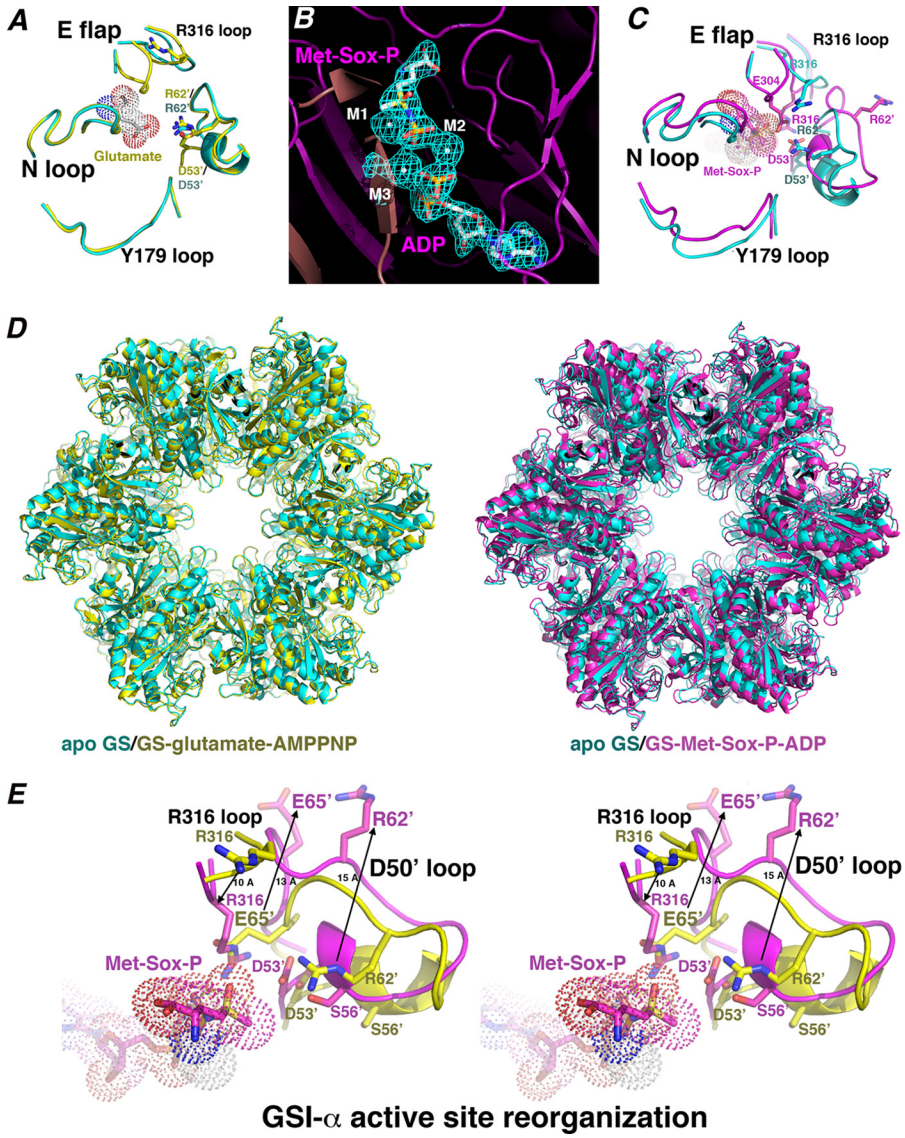

FIGURE 3. ***B. subtilis* GS active site architecture, substrate binding, and transition state conformational changes.** *A*, *close-up* of key active site loop regions in the apo-GS (*cyan*) and glutamate-bound GS structures (*yellow*). The apo-Glu flap is mostly disordered, whereas in the glutamate-bound structure, the Glu flap backbone atoms are resolved. No large structural changes are noted between key loops. *B*, initial $F_o - F_c$ map of the GS·transition state complex contoured at 3.5 σ calculated before the addition of Met-Sox-P, ADP, and metal ions (to 2.58 Å). *C*, *close-up* of the active site regions around key loops (as in *A*) after superimposition of the apo-state (*cyan*) and transition state (*magenta*) complexes. Large structural changes in the loops occur upon transition state formation, especially in the $Asp^{50'}$ loop. *D*, superimposition of the apo-GS dodecamer (*cyan*) onto the glutamate·AMPPCP-bound (*yellow*) and Met-Sox-P·ADP-bound (*magenta*) forms. *E*, *stereo view* showing superimposition of the substrate-bound form of GS (*yellow*) and the transition state complex (*magenta*), highlighting critical active site loop rearrangements that provide proper active site architecture for catalysis during formation of the transition state. Most notable are the complete ejection of $Arg^{62'}$ and $Glu^{65'}$, which permit adjustment of $Asp^{53'}$ and Arg^{316} into the pocket for catalysis. The extent of the structural changes is indicated by *arrows* and distances in Å.

organization of catalytic residues. This is largely due to the deep insertion of the latch, in particular residues $Arg^{62'}$ and $Glu^{65'}$, into the neighboring active site of each subunit. $Arg^{62'}$ blocks and prevents the correct positioning of the catalytic $Asp^{53'}$ as well as $Ser^{56'}$, which stabilizes the Glu flap. Moreover, the side chain of $Glu^{65'}$ overlaps the location of the key catalytic arginine, Arg^{316}, which assists in phosphoryl transfer. In fact, in the apo- and substrate-bound GSI-α structures, the side chain of Arg^{316} is located entirely outside the active site.

The non-optimal active site organization in the apo- and substrate-bound GSI-α structures suggests that either a different catalytic mechanism may be at play in GSI-α and GSI-β proteins or that significant structural changes must occur during catalysis. To address this question, we generated a GSI-α·transition state complex by reacting the protein with Met-Sox, ATP, and Mg^{2+} and crystallized and solved the structure to R_{work}/R_{free} values of 20.3%/23.2% to 2.58 Å (see "Experimental Procedures") (Table 1). Met-Sox-P mimics the GS transition state as its methyl group occupies the ammonium substrate binding site (8). Thus, the Met-Sox-P adduct forms a stable complex with the enzyme that precludes the last step, which is release of the phosphate from the intermediate and concomitant abstraction of the proton from the intermediate γ-amino group by Glu flap residue Glu^{304}. The structure revealed that the expected catalysis had occurred, leading to Met-Sox-P and ADP creation (Fig. 3*B*).

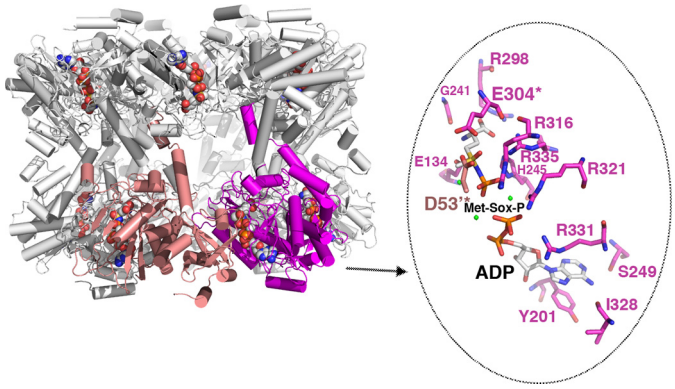

FIGURE 4. **Structure of the GSI-α Met-Sox-P·ADP complex and *close-up* of contacts to the transition state.** The structure of the dodecamer is displayed as *ribbons* with one subunit *colored magenta* and the neighboring subunit *colored salmon*. The Met-Sox-P and ADP molecules in each active site are shown as *CPK*. Note that there is a dodecamer in the crystallographic asymmetric unit, and each active site (formed between subunits) has generated the identical transition state with the same contacts. One active site (*between* the *magenta* and *salmon* subunits) is highlighted, and key residues that contact Met-Sox-P and ADP are shown as *sticks* (*enlarged view* to the *right*). The key catalytic residues Asp^{53} and Glu^{304} are *labeled* and highlighted with *asterisks*. Magnesium ions are *colored green*.

GS enzymes all utilize two Mg^{2+} ions to aid substrate binding, transfer of the phosphate group, and structural stability. In the GSI-α·transition state structure, a third metal ion is found, which probably functions in neutralizing the negative charge arising from the intermediate. A similarly located metal ion was identified in the *M. tuberculosis* GSI-β·Met-Sox-P and maize GSII·phosphinothricin structures (5, 8). Contacts to the adenine and ribose moieties of ADP in the transition state complex are essentially identical to those made to AMPPCP. In the transition state complex, however, the phosphate groups are rotated into the active site near the Met-Sox-P and are contacted by Arg^{321} and Arg^{331} as well as a Mg^{2+} ion. The β-phosphate lies close to the phosphate transferred to Met-Sox to form Met-Sox-P. There are numerous contacts from GS to the Met-Sox-P. Arg^{298} interacts with the carboxyl moiety, and the Met-Sox-P amide nitrogen interacts with the Glu^{134} side chain as well as the carbonyl of Gly^{241}. The Met-Sox-P phosphate moiety is surrounded by multiple basic residues, including Arg^{316}, Arg^{321}, Arg^{335}, and His^{245} (Figs. 3,*C–E,* and 4). Glu flap residue Glu^{304} contacts $Asp^{53'}$ and is within close distance to the Met-Sox-P methyl group. The Glu^{304}-$Asp^{53'}$ interaction probably helps to stabilize and shield the Met-Sox-P from attack by bulk solvent as well as facilitating proton abstraction of the ammonium to form ammonia. The resultant ammonia is then in an ideal position to attack the γ-glutamyl phosphate intermediate. Hence, the GSI-α·Met-Sox-P·ADP complex mimics the tetrahedral adduct before the generation of glutamine and inorganic phosphate products.

Comparison of the transition state structure with the apo- and substrate-bound forms revealed dramatic conformational changes, consonant with the finding that the residues in the transition state structure are optimally positioned for catalysis. The largest structural changes are located on the active site loop regions (r.m.s. deviations of apo-/substrate-bound *versus* Met-Sox-bound subunits = 1.8–2.0 Å, whereas the r.m.s. deviations are 0.8 Å when the active site loops are not included). Moreover, superimposition of the transition state dodecamer onto the apo- or substrate-bound dodecamers results in r.m.s. deviations of 2.5–3.0 Å, indicating that the catalytically induced structural changes are transmitted between subunits, leading to significant alterations in the overall dodecamer structure (Fig. 3*D*). Although all of the GSI-α active site loops are altered upon transition state formation, residues in the $Asp^{50'}$ loop undergo the most dramatic structural rearrangements (r.m.s. deviations = 3.7–4.0 Å for superimposition of the $Asp^{50'}$ loops of the transition state and glutamate-bound structures). As noted, the $Asp^{50'}$ loop is wedged into the active site in apo- and substrate-bound structures, preventing an optimal configuration of catalytic residues. The restructuring of the active site that takes place during catalysis results in a functional arrangement of catalytic residues (Fig. 3, *C* and *E*). These extensive structural changes include the unfolding of one turn of the helix from residue 53 to 59. The structural changes in the $Asp^{50'}$ loop lead to the expulsion of $Glu^{65'}$ and $Arg^{62'}$ more than 10 Å from the active site to the solvent-exposed surface of the dodecamer (Fig. 3*E*). Concomitantly, the Arg^{316} loop moves by ~10 Å, resulting in relocation of the Arg^{316} side chain into the position vacated by $Glu^{65'}$. These alterations create an active site organization that allows GSI-α to employ the same general catalytic mechanism used by all characterized GS proteins (3).

Demonstration that B. subtilis GS Is Cooperative Using Mixed Oligomers—The structural changes that take place during GSI-α catalysis are found in all the active sites and result in an altered dodecamer structure, suggesting that the enzyme may be cooperative, whereby binding and catalysis at one active site is affected by adjacent subunits. Such cooperativity has been indicated by previous studies revealing active site coupling with *E. coli* GS (45). However, to directly assess GSI-α cooperativity, we developed a mixed dodecamer assay. Previous studies showed that single E304A and A305G mutations abrogated GS activity (40). Thus, in this assay, WT GS subunits were mixed with inactive, double GS(E304A/A305G) mutant subunits in the presence of 2 M urea, allowing subunit exchange. The mixture was then dialyzed into urea free buffer resulting in the formation of mixed oligomers. 2 M urea treatment did not cause denaturation as assessed by circular dichroism but broke up subunit-subunit interactions (see "Experimental Procedures") (Fig. 5). To assay possible effects of urea treatment on GS function, we first tested the activity of WT GS and WT GS that had undergone the identical urea treatment as the mixed oligomer. As shown in Table 4, this procedure had no effect on GS enzyme activity. If GSI-α is not cooperative, a mixed WT GS·GS(E304A/A305G)-containing dodecamer should display either WT or only slightly reduced enzyme activity. By contrast, if the dodecamer is cooperative, then incorporation of even a few GS(E304A/A305G) subunits into the dodecamer should impair or abrogate activity for a cooperative enzyme. The mixture used in the assay depicted in Fig. 5 contained between a 3- and 4-fold excess of the WT protein (lower molecular weight band) compared with the mutant. Thus, this experiment provided a strong test case of cooperativity. Even under these conditions, where there is far less mutant than WT, the activity was abrogated, supporting the hypothesis that the dodecamer is cooperative (Table 4).

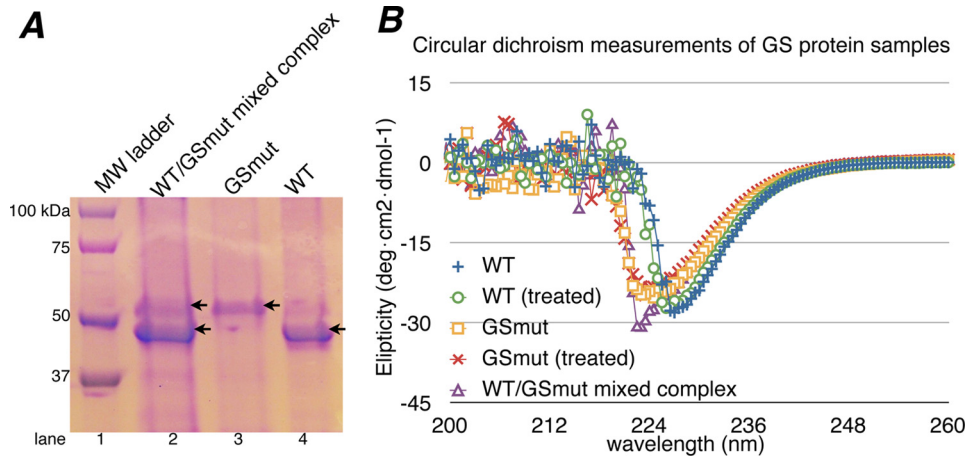

FIGURE 5. *A*, SDS-PAGE of GS proteins used for mixed dodecamer/cooperativity assays. *Lanes 3* and *4*, the E304A/A305G and WT protein samples, respectively. *Lane 2*, WT GS/GS(E304A-A305G) mixed complex after urea treatment, urea removal, and purification. *B*, circular dichroism measurements of GS proteins before and after urea treatment. Overall, the spectrum of treated and untreated WT GS, GS(E304A/A305G), and the mixed complex are indicative of well folded α-β proteins (note the peaks in the 220–230 nm range). This demonstrates that urea treatment did not affect the secondary structures or overall folds of the GS proteins.

TABLE 4
Glutamine synthetase cooperativity assay

Enzyme	Glutamine synthetase-specific activity		
	Forward reaction (biosynthetic)		
	Mg^{2+}-dependent[a]	Mn^{2+}-dependent[a]	Reverse reaction (transferase)[a]
WT	0.406 ± 0.035	0.187 ± 0.009	9.555 ± 0.490
WT (treated)[b]	0.413 ± 0.019	0.193 ± 0.012	9.643 ± 0.422
GS(E304A/A305G)	0.003 ± 0.001	0.005 ± 0.004	0.029 ± 0.007
GS(E304A/A305G) (treated)[b]	0.003 ± 0.001	0.005 ± 0.002	0.038 ± 0.014
WT-E304A/A305G mixed complex	0.005 ± 0.001	0.006 ± 0.004	0.037 ± 0.012

[a] 1 unit of GS activity corresponds to the ATP/ADP-dependent formation of 1 nmol of γ-glutamylhydroxamate min^{-1}.
[b] Samples were treated with 2 M urea then dialyzed to remove urea (see "Experimental Procedures").

Molecular Basis for GSI-α-specific Gln Feedback Inhibition—GSI-α enzymes are distinct from their GSI-β counterparts in that they are feedback-inhibited by the reaction product, Gln. Previous GSI-β-Gln structures showed no interactions between Gln and side chains of the Glu flap, and the bound glutamine and Glu flap were largely disordered in the structure (3). Indeed, this Glu flap flexibility was suggested as being important in facile product release following catalysis. The finding that GSI-α enzymes are feedback-inhibited by Gln suggests that differences must exist in GSI-Gln isoenzyme structures. It also indicates that important distinctions must be present between GSI-α-Glu and GS-α-Gln structures. Understanding the structural basis for GSI-α-Gln feedback inhibition is crucial, because this form of the enzyme serves as a key nexus in the Bacilli nitrogen regulation pathway (29–31). Thus, we next determined structures of *B. subtilis* GS·Gln-Mg^{2+} complexes. Two structures were obtained using different crystallization conditions (see "Experimental Procedures") (Table 2). The two structures are identical and reveal that Gln binds within the Glu flap pocket in a similar location as the substrate glutamate (Fig. 6*A*). However, there are striking differences between the Gln-bound and Glu-bound states. Unlike the Glu-bound state, in the Gln-bound structure, both the side chain and backbone atoms of Glu flap residues are well ordered; the *B*-factors (average) for Glu flap residues in the Gln-bound structure are 35.9 $Å^2$ compared with 85.0 $Å^2$ for the glutamate-bound form, and the *B*-factors (average) for the glutamines are

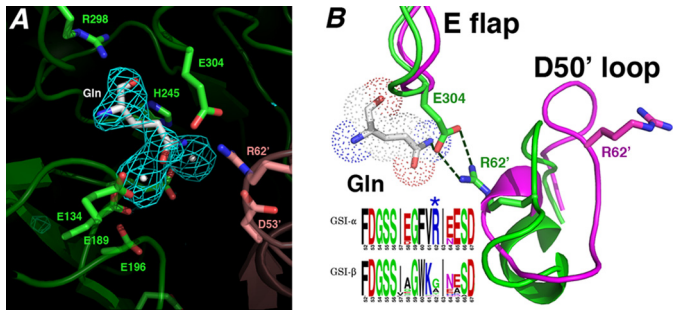

FIGURE 6. **Structural basis for GSI-α-specific Gln feedback inhibition.** *A*, initial $F_o - F_c$ map calculated before the addition of glutamine and metal ions and contoured at 3.2 σ (to 2.95 Å). *B*, superimposition of active site loops of the glutamine-bound state (*green*) and the transition state complex (*magenta*). The Gln-bound active site loops adopt structures similar to apo- and substrate-bound except that the Glu flap (*E flap*) is well ordered, and the Glu flap residue Glu^{304} hydrogen-bonds to the Gln as well as the GSI-α-specific residue from the $Asp^{50'}$ loop (*D50′ loop*), $Arg^{62'}$. Notably, GSI-β enzymes are not feedback-inhibited by Gln. As shown by the *logo*, GSI-β enzymes all lack the key $Arg^{62'}$ residue, explaining why they are not subject to Gln feedback inhibition (in the *logo*, residues are *colored* according to type, basic in *blue*, acidic in *red*, hydrophobic in *black*, and glycine/serine in *green*).

33.0 $Å^2$ (Table 3). In fact, although not directly comparable due to their differing resolutions, the *B*-factors of the Glu flap residues in the Gln-bound structures are on par with those in the transition state structure (which have *B*-factors (average) = 24.0 $Å^2$ for Glu flap residues and 20.0 and 20.3 $Å^2$ for ADP and Met-Sox-P, respectively) (Table 3).

In the GSI-α-Gln structures, the $Asp^{50'}$ loop adopts the same conformation as that observed in the apo- and substrate-bound

GSI-α forms (Figs. 6*B* and 7). Remarkably, however, in the GS-Gln structure, Arg^{62} plays a central role in Gln binding and, hence, Gln feedback inhibition. Specifically, the $Arg^{62'}$ side chain hydrogen-bonds with the key catalytic residue from the Glu flap, Glu^{304} (Fig. 6*B*). The stabilized Glu^{304} also makes a tight hydrogen bond to the glutamine Nϵ atom. This intimate hydrogen bond network ties the Glu flap closed, explaining its well ordered state in this structure (Fig. 6*B*). The vital role played by Arg^{62} in Gln feedback inhibition probably explains why, unlike GSI-β enzymes, the GSI-α $Asp^{50'}$ loop adopts distinct structures in different states. $Asp^{50'}$ loop insertion into the active site in GSI-α is critical for Gln feedback inhibition, but it can then be readily ejected in the absence of the Gln-specific hydrogen bond network to allow catalysis. In this way, the $Asp^{50'}$ loop acts as a GSI-α-specific regulatory trigger.

The finding that Glu^{304} directly interacts with Gln provides a molecular explanation for previous studies showing that E304D or E304A mutants were defective in Gln feedback inhibition (40). The intricate Arg^{62}-Glu^{304}-Gln hydrogen bond linkage also explains why GSI-α, but not GSI-β, enzymes are feedback-inhibited by Gln because sequence alignments of GS proteins show that Arg^{62} is completely conserved in GSI-α enzymes but not GSI-β enzymes, where this position is typically Gly or Ala (Fig. 6*B*). Thus, these structures demonstrate that *B. subtilis* GS uses a residue found only in GSI-α enzymes, Arg^{62}, along with a conserved catalytic residue (Glu^{304}) to mediate glutamine binding. The structures also reveal the basis for Gln feedback inhibition, because the $Arg^{62'}$-Glu^{304}-Gln hydrogen bond network locks the Glu flap in a closed state, preventing Gln release, substrate binding and catalysis.

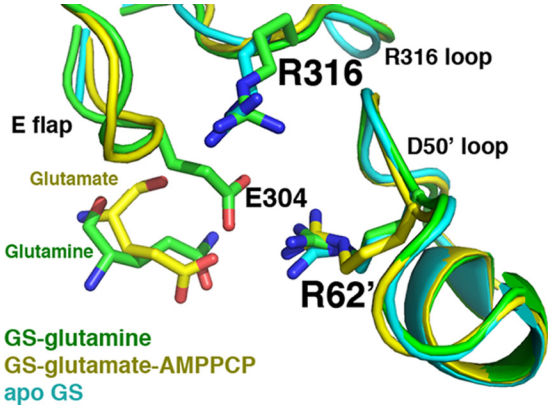

FIGURE 7. **The GS·glutamine structure active site is similar to that of the apo- and substrate-bound forms.** Superimposition of the apo-, glutamate-AMPPCP, and glutamine-bound GSI-α structures, focusing on key active site loops. The apo-structure is *colored cyan*, the glutamate-AMPPCP-bound structure is *yellow*, and the glutamine-bound structure is *green*. The active site loops adopt essentially the same conformation. The Glu flap in the apo-state is mostly disordered, whereas backbone atoms of the Glu flap in the substrate-bound state are visible (but not side chains), and in the glutamine-bound form, the Glu flap is as well ordered as in the transition state.

The Role of Arg^{62} in GS Activity and Regulation; Kinetic, Enzymological, and in Vivo Studies—Our structures indicate that Arg^{62} plays a key role in GSI-α-specific Gln feedback inhibition. The structures also suggest that Arg^{62} is not involved in catalysis and, in fact, must be ejected from the active site during transition state formation. To test these structure-based hypotheses, an R62A mutant was constructed. The purified R62A enzyme had only small differences (less than 2-fold) in its steady-state kinetic constants compared with WT, indicating that it does not play a significant role in substrate binding or catalysis, consistent with our structural data (Table 5). Unlike the E304A substitution in GS, the R62A replacement did not increase the K_m for ammonium (Table 5). This result is again consistent with the structural data and argues that Arg^{62} is not part of the ammonium substrate binding site. In contrast to E304A, which is highly resistant to Met-Sox inhibition, the R62A enzyme has a sensitivity to Met-Sox that is similar to that of WT GS (Table 6). These data, again, support the idea that Arg^{62} is not involved in the GS reaction mechanism. Strikingly, however, and consistent with our structural findings, the R62A mutant was highly resistant to Gln feedback inhibition (Table 6). The R62A substitution was also found to increase the resistance to AMP inhibition. We have argued previously that there is an interdependence between the glutamate (glutamine) and ATP (AMP) binding sites (40). The activities of the nitrogen transcription factors TnrA and GlnR are regulated by the feedback-inhibited form of GS (29–31). TnrA- and GlnR-regulated genes were shown previously to be expressed constitutively in mutants encoding feedback-resistant GS enzymes (29–31). The contribution of the GS Arg^{62} residue to the *in vivo* regulation of TnrA and GlnR was assessed by constructing a *B. subtilis* mutant containing an R62A substitution in the chromosomal GS gene (*glnA*) (see "Experimental Procedures") (40). Gene reg-

TABLE 6

Sensitivities of wild-type and mutant GS proteins to inhibition

The IC_{50} is the inhibitor concentration that reduces enzymatic activity by 50%. The Mg^{2+}-dependent biosynthetic reaction was used to measure the inhibition. All values are the averages of at least two determinations. The S.E. values were less than 10% for all values. The values for the wild-type and E304A enzymes are taken from Ref. 40.

Enzyme	IC_{50}		
	Glutamine	AMP	Met-Sox
		mM	
Wild type	2.4	0.5	0.13
R62A	>140	20	0.19
E304A	>140	>30	26

TABLE 5

Enzymatic constants for wild-type and mutant GS proteins

The kinetic constants were determined for the Mg^{2+}-dependent biosynthetic reaction. All assays were performed at least twice. The uncertainty is the S.E. from the nonlinear regression analysis of the data.

Enzyme	K_m				V_{max}
	Glutamate	ATP	Ammonium	Hydroxylamine	
			mM		*μmol/min/mg*
Wild type	27 ± 2	2.4 ± 0.1	0.18 ± 0.03	0.83 ± 0.07	3.7 ± 0.2
R62A	14 ± 2	2.3 ± 0.3	0.34 ± 0.05	1.4 ± 0.2	2.9 ± 0.1
E304A	3.4 ± 0.2	1.2 ± 0.1	32 ± 2	0.68 ± 0.09	1.3 ± 0.1

TABLE 7

TnrA- and GlnR-dependent gene regulation

β-Galactosidase activity was determined in extracts of cells harvested during exponential growth in glucose minimal medium containing glutamate plus casamino acids or glutamate as the respective nitrogen sources for excess and limiting nitrogen conditions. Each value is the mean of at least two independent determinations and is reproducible to within 10% (S.E.) of the mean value.

	TnrA-dependent regulation; β-galactosidase activity from an *amtB-lacZ* fusion		GlnR-dependent regulation; β-galactosidase activity from a *glnRA-lacZ* fusion	
Relevant genotype	Excess nitrogen	Limited nitrogen	Excess nitrogen	Limited nitrogen
	nmol/min/mg		*nmol/min/mg*	
Wild type	14	140	17	30
glnA(R62A)	100	83	38	34

ulation by TnrA and GlnR was abolished in cells encoding GS with an R62A mutation (Table 7). These results indicate that the *glnA*(*R62A*) mutant has the *in vivo* phenotypes expected for a strain encoding for feedback-resistant GS enzyme.

In conclusion, we have captured all key catalytic and regulatory states of the *B. subtilis* GSI-α enzyme. Surprisingly, these structures reveal heretofore unseen large structural changes during catalysis. GSI-α enzymes are also distinct among GSs in being feedback-inhibited by the product, Gln. Remarkably, our work demonstrates that the catalytic and regulatory features of GSI-α are linked. Specifically, Gln feedback inhibition arises from a hydrogen bond network between Gln, the active site Glu^{304}, and a GSI-α-specific residue, $Arg^{62\prime}$, from an adjacent subunit. Notably, $Arg^{62\prime}$ is ejected from the active site as part of the GSI-α active site reorganization during catalysis. These key Arg^{62} roles were supported by biochemical and *in vivo* studies; mutation of Arg^{62} to alanine eliminates Gln feedback inhibition but does not affect catalysis. The extensive conformational changes that take place during catalysis also suggest a cooperative catalytic mechanism, which was supported by a mixed dodecamer enzyme assay. Due to its critical role in nitrogen metabolism, GS is an attractive and validated target for drug design against pathogenic bacteria. The isoenzyme-specific glutamine interaction network uncovered here presents a promising point of intervention in the development of highly specific inhibitors in the treatment of Gram-positive pathogenic bacteria.

Acknowledgments—We dedicate this work to our colleague and dear friend Dr. David Murray, who spearheaded the GS work as a graduate student and sadly passed away. We thank the Advanced Light Source (ALS) and their support staff. The ALS is supported by the Director, Office of Science, Office of Basic Energy Sciences, and Material Science Division of the United States Department of Energy at the Lawrence Berkeley National Laboratory.

REFERENCES

1. Magasanik, B. (1993) The regulation of nitrogen utilization in enteric bacteria. *J. Cell. Biochem.* **51,** 34–40
2. Pesole, G., Bozzetti, M. P., Lanave, C., Preparata, G., and Saccone, C. (1991) Glutamine synthetase gene evolution. A good molecular clock. *Proc. Natl. Acad. Sci. U.S.A.* **88,** 522–526
3. Eisenberg, D., Gill, H. S., Pfluegl, G. M., and Rotstein, S. (2000) Structure-function relationships of glutamine synthetases. *Biochim. Biophys. Acta* **1477,** 122–145
4. Krajewski, W. W., Collins, R., Holmberg-Schiavone, L., Jones, T. A., Karlberg, T., and Mowbray, S. L. (2008) Crystal structures of mammalian glutamine synthetases illustrate substrate-induced conformational changes and provide opportunities for drug and herbicide design. *J. Mol. Biol.* **375,** 217–228
5. Unno, H., Uchida, T., Sugawara, H., Kurisu, G., Sugiyama, T., Yamaya, T., Sakakibara, H., Hase, T., and Kusunoki, M. (2006) Atomic structure of plant glutamine synthetase. A key enzyme for plant productivity. *J. Biol. Chem.* **281,** 29287–29296
6. van Rooyen, J. M., Abratt, V. R., Belrhali, H., and Sewell, T. (2011) Crystal structure of the type III glutamine synthetase. Surprising reversal of the inter-ring interface. *Structure* **19,** 471–483
7. Almassy, R. J., Janson, C. A., Hamlin, R., Xuong, N. H., and Eisenberg, D. (1986) Novel subunit-subunit interactions in the structure of glutamine synthetase. *Nature* **323,** 304–309
8. Krajewski, W. W., Jones, T. A., and Mowbray, S. L. (2005) Structure of *Mycobacterium tuberculosis* glutamine synthetase in complex with a transition-state mimic provides functional insights. *Proc. Natl. Acad. Sci. U.S.A.* **102,** 10499–10504
9. Nilsson, M. T., Krajewski, W. W., Yellagunda, S., Prabhumurthy, S., Chamarahally, G. N., Siddamadappa, C., Srinivasa, B. R., Yahiaoui, S., Larhed, M., Karlén, A., Jones, T. A., and Mowbray, S. L. (2009) Structural basis for inhibition of *Mycobacterium tuberculosis* glutamine synthetase by novel ATP-competitive inhibitors. *J. Mol. Biol.* **393,** 504–513
10. Liaw, S. H., and Eisenberg, D. (1994) Structural model for the reaction mechanism of glutamine synthetase, based on five crystal structures of enzyme-substrate complexes. *Biochemistry* **33,** 675–681
11. Liaw, S. H., Jun, G., and Eisenberg, D. (1994) Interactions of nucleotides with fully unadenylylated glutamine synthetase from *Salmonella typhimurium*. *Biochemistry* **33,** 11184–11188
12. Liaw, S. H., Kuo, I., and Eisenberg, D. (1995) Discovery of the ammonium substrate site on glutamine synthetase, a third cation binding site. *Protein Sci.* **4,** 2358–2365
13. Gill, H. S., and Eisenberg, D. (2001) The crystal structure of phosphinothricin in the active site of glutamine synthetase illuminates the mechanism of enzymatic inhibition. *Biochemistry* **40,** 1903–1912
14. Brown, J. R., Masuchi, Y., Robb, F. T., and Doolittle, W. F. (1994) Evolutionary relationships of bacterial and archaeal glutamine synthetase genes. *J. Mol. Evol.* **38,** 566–576
15. Deuel, T. F., and Prusiner, S. (1974) Regulation of glutamine synthetase from *Bacillus subtilis* by divalent cations, feedback inhibitors, and L-glutamine. *J. Biol. Chem.* **249,** 257–264
16. Midelfort, C. F., and Rose, I. A. (1976) A stereochemical method for detection of ATP terminal phosphate transfer in enzymatic reactions. Glutamine synthetase. *J. Biol. Chem.* **251,** 5881–5887
17. Wedler, F. C., and Boyer, P. D. (1972) Substrate binding and reaction intermediates of glutamine synthetase (*Escherichia coli* W) as studied by isotope exchanges. *J. Biol. Chem.* **247,** 984–992
18. Wedler, F. C., and Horn, B. R. (1976) Catalytic mechanisms of glutamine synthetase enzymes. Studies with analogs of possible intermediates and transition states. *J. Biol. Chem.* **251,** 7530–7538
19. Deuel, T. F., and Stadtman, E. R. (1970) Some kinetic properties of *Bacillus subtilis* glutamine synthetase. *J. Biol. Chem.* **245,** 5206–5213
20. Purich, D. L. (1998) Advances in the enzymology of glutamine synthesis. *Adv. Enzymol. Relat. Areas Mol. Biol.* **72,** 9–42
21. Deuel, T. F., Ginsburg, A., Yeh, J., Shelton, E., and Stadtman, E. R. (1970) *Bacillus subtilis* glutamine synthetase. Purification and physical characterization. *J. Biol. Chem.* **245,** 5195–5205
22. Harth, G., and Horwitz, M. A. (1999) An inhibitor of exported *Mycobacterium tuberculosis* glutamine synthetase selectively blocks the growth of pathogenic mycobacteria in axenic culture and in human monocytes. Extracellular proteins as potential novel drug targets. *J. Exp. Med.* **189,** 1425–1436
23. Fisher, S. H. (1999) Regulation of nitrogen metabolism in *Bacillus subtilis*. Vive la difference! *Mol. Microbiol.* **32,** 223–232
24. Fisher, S. H., and Sonenshein, A. L. (1984) *Bacillus subtilis* glutamine synthetase mutants pleiotropically altered in glucose catabolite repression. *J. Bacteriol.* **157,** 612–621
25. Schreier, H. J., Brown, S. W., Hirschi, K. D., Nomellini, J. F., and Sonen-

shein, A. L. (1989) Regulation of *Bacillus subtilis* glutamine synthetase gene expression by the product of the *glnR* gene. *J. Mol. Biol.* **210,** 51–63
26. Wray, L. V., Jr., Ferson, A. E., Rohrer, K., and Fisher, S. H. (1996) TnrA, a transcription factor required for global nitrogen regulation in *Bacillus subtilis*. *Proc. Natl. Acad. Sci. U.S.A.* **93,** 8841–8845
27. Ferson, A. E., Wray, L. V. Jr., and Fisher, S. H. (1996) Expression of the *Bacillus subtilis gabP* gene is regulated independently in response to nitrogen and amino acid availability. *Mol. Microbiol.* **22,** 693–701
28. Fisher, S. H., and Wray, L. V. Jr. (2002) Bacillus subtilis 168 contains two differentially regulated genes encoding L-asparaginase. *J. Bacteriol.* **184,** 2148–2154
29. Wray, L. V., Jr., Zalieckas, J. M., and Fisher, S. H. (2001) *Bacillus subtilis* glutamine synthetase controls gene expression through a protein-protein interaction with transcription factor TnrA. *Cell* **107,** 427–435
30. Wray, L. V., Jr., and Fisher, S. H. (2008) *Bacillus subtilis* GlnR contains an autoinhibitory C-terminal domain required for the interaction with glutamine synthetase. *Mol. Microbiol.* **68,** 277–285
31. Fisher, S. H., and Wray, L. V. Jr., (2008) *Bacillus subtilis* glutamine synthetase regulates its own synthesis by acting as a chaperone to stabilize GlnR-DNA complexes. *Proc. Natl. Acad. Sci. U.S.A.* **105,** 1014–1019
32. Wray, L. V., Jr., and Fisher, S. H. (2005) A feedback-resistant mutant of *Bacillus subtilis* glutamine synthetase with pleiotropic defects in nitrogen-regulated gene expression. *J. Biol. Chem.* **280,** 33298–33304
33. Reitzer, L. (2003) Nitrogen assimilation and global regulation in *Escherichia coli*. *Annu. Rev. Microbiol.* **57,** 155–176
34. Shapiro, B. M., Kingdon, H. S., and Stadtman, E. R. (1967) Regulation of glutamine synthetase. VII. Adenylyl glutamine synthetase. A new form of the enzyme with altered regulatory and kinetic properties. *Proc. Natl. Acad. Sci. U.S.A.* **58,** 642–649
35. Shapiro, B. M., and Stadtman, E. R. (1968) 5′-adenylyl-*O*-tyrosine. The novel phosphodiester residue of adenylylated glutamine synthetase from *Escherichia coli*. *J. Biol. Chem.* **243,** 3769–3771
36. Mehta, R., Pearson, J. T., Mahajan, S., Nath, A., Hickey, M. J., Sherman, D. R., and Atkins, W. M. (2004) Adenylylation and catalytic properties of *Mycobacterium tuberculosis* glutamine synthetase expressed in *Escherichia coli versus* mycobacteria. *J. Biol. Chem.* **279,** 22477–22482
37. Brünger, A. T., Adams, P. D., Clore, G. M., DeLano, W. L., Gros, P., Grosse-Kunstleve, R. W., Jiang, J. S., Kuszewski, J., Nilges, M., Pannu, N. S., Read, R. J., Rice, L. M., Simonson, T., and Warren, G. L. (1998) Crystallography and NMR system. A new software suite for macromolecular structure determination. *Acta Crystallogr. D Biol. Crystallogr.* **54,** 905–921
38. Afonine, P. V., Grosse-Kunsteve, R. W., Echols, N., Head, J. J., Moriarty, N. E., Mustyakimov, M., Terwilliger, T. C., Urzhumtsev, A., Zwart, P. H., and Adams, P. D. (2012) Towards automated crystallographic structure refinement with phenix.refine. *Acta Crystallogr. D Biol. Crystallogr.* **68,** 352–367
39. Jones, T. A., Zou, J. Y., Cowan, S. W., and Kjeldgaard, M. (1991) Improved methods for building protein models in electron density maps and the location of errors in these models. *Acta Crystallogr. A* **47,** 110–119
40. Wray, L. V. Jr., and Fisher, S. H. (2010) Functional roles of the conserved Glu^{304} loop of *Bacillus subtilis* glutamine synthetase. *J. Bacteriol.* **192,** 5018–5025
41. Neidhardt, F. C., Bloch, P. L., and Smith, D. F. (1974) Culture medium for enterobacteria. *J. Bacteriol.* **119,** 736–747
42. Atkinson, M. R., Wray, L. V. Jr., and Fisher, S. H. (1990) Regulation of histidine and proline degradation enzymes by amino acid availability in *Bacillus subtilis*. *J. Bacteriol.* **172,** 4758–4765
43. Gawronski, J. D., and Benson, D. R. (2004) Microtiter assay for glutamine synthetase biosynthetic activity using inorganic phosphate detection. *Anal. Biochem.* **327,** 114–118
44. Weisbrod, R. E., and Meister, A. (1973) Studies on glutamine synthetase from *Escherichia coli*. Formation of pyrrolidone carboxylate and inhibition by methionine sulfoximine. *J. Biol. Chem.* **248,** 3997–4002
45. Rhee, S. G., Chock, P. B., Wedler, F. C., and Sugiyama, Y. (1981) Subunit interaction in unadenylated glutamine synthetase from *Escherichia coli*. *J. Biol. Chem.* **256,** 644–648
46. Fisher, S. H., and Wray, L. V. Jr. (2009) Novel trans-acting *Bacillus subtilis glnA* mutations that deprepress *glnRA* expression. *J. Bacteriol.* **191,** 2485–2492
47. DeLano, W. L. (2010) *The PyMOL Molecular Graphics System*, version 1.3r1, Schrödinger, LLC, New York